

# RSC Advances



This is an *Accepted Manuscript*, which has been through the Royal Society of Chemistry peer review process and has been accepted for publication.

*Accepted Manuscripts* are published online shortly after acceptance, before technical editing, formatting and proof reading. Using this free service, authors can make their results available to the community, in citable form, before we publish the edited article. This *Accepted Manuscript* will be replaced by the edited, formatted and paginated article as soon as this is available.

You can find more information about *Accepted Manuscripts* in the [Information for Authors](#).

Please note that technical editing may introduce minor changes to the text and/or graphics, which may alter content. The journal's standard [Terms & Conditions](#) and the [Ethical guidelines](#) still apply. In no event shall the Royal Society of Chemistry be held responsible for any errors or omissions in this *Accepted Manuscript* or any consequences arising from the use of any information it contains.

## ARTICLE

Cite this: DOI:  
10.1039/x0xx00000x

## Effects of alkaline-earth oxides on the performance of CuO-ZrO<sub>2</sub> catalyst for methanol synthesis via CO<sub>2</sub> hydrogenation

Received 00th January 2015,  
Accepted 00th January 2015

Chenglin Zhong, Xiaoming Guo,\* Dongsen Mao, Song Wang, Guisheng Wu and Guanzhong Lu

DOI: 10.1039/x0xx00000x

[www.rsc.org/](http://www.rsc.org/)

CuO-ZrO<sub>2</sub> catalysts doped with alkaline-earth oxides were prepared by a urea-nitrate combustion method. The catalysts were characterized with N<sub>2</sub> adsorption, N<sub>2</sub>O titration, XRD, H<sub>2</sub>-TPR, XPS and CO<sub>2</sub>-TPD techniques and tested for methanol synthesis from CO<sub>2</sub> hydrogenation. With the incorporation of alkaline-earth oxides, the copper surface area increases remarkably, whereas the reducibility of CuO in catalyst decreases. The doping of alkaline-earth oxides leads to an increase in the strength and contribution of the strong basic site on catalyst surface. The results of catalytic test indicate that the conversion of CO<sub>2</sub> depends not only on the copper surface area but also on the reducibility of CuO in catalyst, and the latter is a predominant factor for CaO-, SrO- and BaO-doped CuO-ZrO<sub>2</sub> catalyst. The selectivity to methanol is related to the basicity of catalyst. Moreover, the influence of the doping amount of MgO on the properties of CuO-ZrO<sub>2</sub> was investigated, and the optimum catalytic activity is obtained as the amount of MgO doping is 5 mol%.

### 1. Introduction

Carbon dioxide has been widely regarded as the main greenhouse gas, linked to the problem of global warming. Carbon dioxide is also available as an infinite carbon source. Efficient conversion of carbon dioxide is of great significance from the viewpoint of environmental protection and effective utilization of carbon resources. Most of the existing research focuses on CO<sub>2</sub> hydrogenation to methanol since methanol is an important feedstock for the organic chemical industry and a potential alternative to fossil fuels<sup>1,2</sup>. Based on the great significance of methanol synthesis from CO<sub>2</sub> hydrogenation, the concept of “methanol economy” was proposed by Nobel laureate Olah<sup>3</sup>.

It is well documented that CuO-ZrO<sub>2</sub> based catalysts exhibit a high catalytic activity for methanol synthesis from CO<sub>2</sub> hydrogenation<sup>4-9</sup>. To further improve the performance of CuO-ZrO<sub>2</sub> based catalyst, a variety of promoters were added, and the effects of these promoters were estimated<sup>10-14</sup>. For example, Kilo et al.<sup>10</sup> studied the effects of Cr and Mn oxide on the structural and catalytic properties of CuO-ZrO<sub>2</sub>. They found

that the presence of Cr or Mn retarded the sintering of copper crystallite and stabilized the amorphous state of zirconia, thus resulting in an increased thermal stability of catalysts. Słoczyński et al.<sup>11,12</sup> investigated a series of CuO-ZnO-ZrO<sub>2</sub> catalysts promoted by B, Mn, Mg and Ga, and the results showed that the promoters modified the dispersion of Cu (or the copper surface area), the surface composition of catalyst and the catalytic activity for methanol synthesis. Natesakhawat et al.<sup>13</sup> found that the incorporation of Ga<sub>2</sub>O<sub>3</sub> and Y<sub>2</sub>O<sub>3</sub> into CuO-ZnO-ZrO<sub>2</sub> catalysts enhanced the Cu dispersion and the reducibility of CuO, and a superior methanol synthesis activity was obtained over the doped catalysts. These studies focused on the influences of promoters on the properties of Cu component in catalysts. However, some researches revealed that there were two active centers involved in the catalytic process of CO<sub>2</sub> hydrogenation over the Cu/ZrO<sub>2</sub>-based catalysts<sup>15-17</sup>. One is the Cu component, and the other is the so-called “support” ZrO<sub>2</sub>. The Cu serves to dissociatively adsorb H<sub>2</sub> and to provide a source of atomic hydrogen by spillover, and the ZrO<sub>2</sub> serves to adsorb CO<sub>2</sub> as carbonate-like species which then undergo stepwise hydrogenation to methanol. Such a mechanism is known as “dual-site” mechanism, and it is currently accepted. Because CO<sub>2</sub> is intrinsically an acid molecular, the adsorption and the activation of CO<sub>2</sub> are related closely to the surface basicity of ZrO<sub>2</sub>. In our previous work<sup>18</sup>, the influence of La

Research Institute of Applied Catalysis, School of Chemical and Environmental Engineering, Shanghai Institute of Technology, Shanghai 200235, P. R. China. E-mail: guoxiaoming@sit.edu.cn (X. Guo); Tel/Fax: (+86)-21-60873301.

doping on the catalytic behavior of CuO-ZrO<sub>2</sub> for methanol synthesis was investigated. The results indicate that the conversion of CO<sub>2</sub> depends on the copper surface area, whereas the selectivity to methanol is related to the distribution of basic site on the catalyst surface. Recently, Gao et al. studied a series of promoted CuO-ZnO-Al<sub>2</sub>O<sub>3</sub> catalyst derived from the hydrotalcite-like precursors, and similar results were presented<sup>19,20</sup>. Therefore, both the copper surface area and the surface basicity should be taken into consideration when selecting a suitable promoter for catalyst. Alkaline-earth oxide, a well-known solid base, has been employed in a variety of organic reactions as the main component or promoter of catalyst<sup>21</sup>. Moreover, alkaline-earth oxide exhibits a high thermal stability, which can prevent the agglomeration of catalyst and increase the surface area of catalyst<sup>22,23</sup>. Thus, the introduction of alkaline-earth oxide into CuO-ZrO<sub>2</sub> may regulate the surface basicity and improve the Cu dispersion of catalysts. However, to date, a systematic examination of CuO-ZrO<sub>2</sub> catalyst doped with alkaline-earth oxides for CO<sub>2</sub> hydrogenation is absent.

The primary purpose of the present work is to explore the influence of alkaline-earth oxides (MgO, CaO, SrO and BaO) doping on the properties of CuO-ZrO<sub>2</sub> catalysts. The physicochemical properties of alkaline-earth oxides doped CuO-ZrO<sub>2</sub> catalysts were characterized by XRD, BET, N<sub>2</sub>O titration, TPR, XPS and CO<sub>2</sub>-TPD techniques, and the catalytic activity for methanol synthesis from CO<sub>2</sub> hydrogenation was evaluated. Based on the catalytic mechanism of methanol synthesis, the catalytic activity and selectivity of the doped catalysts were discussed in relation to the physicochemical properties including the copper surface area, the reducibility of CuO and the surface basicity. In addition, the effects of doping amount was emphasized for MgO-doped catalyst.

## 2. Experimental

### 2.1 Catalyst preparation

CuO-ZrO<sub>2</sub> (CZ) and alkaline-earth oxides doped CuO-ZrO<sub>2</sub> (MCZ, M= Mg, Ca, Sr, Ba) catalysts were prepared by the urea-nitrate combustion method. All chemicals used were of analytical reagent grade (Shanghai Chemical Reagent Corporation, Shanghai, China). Firstly, the required amounts of metal nitrates were dissolved in deionized water in a basin to form a mixed solution with a total cation concentration of 3.0 M. Then, the solution of urea (3.5M) was slowly added to the metal nitrate solution under constant stirring. The resulting mixture was kept in an ultrasound bath operating at 47 kHz with a power of 30 W for 0.5 h until a pale-blue slurry was obtained. Afterward, the slurry was transferred to an open muffle furnace preheated at 300 °C. The slurry started boiling with frothing and foaming, and ignition took place. Along with rapid evolution of a large quantity of gases, a foamy, voluminous powder was produced. Because the time for the autoignition was rather short, to remove traces of undecomposed urea, nitrates and their decomposition products, the powder was further calcined in air at 500 °C for 4 h. To

obtain an optimum catalytic performance, the amount of urea used in the combustion process was 50% of the stoichiometric amount, which can be calculated according to propellant chemistry<sup>24</sup>. A more detailed description of the preparation process was given in Ref. [8]. Unsupported CuO powder in this study was prepared via the thermal decomposition of Cu(NO<sub>3</sub>)<sub>2</sub> at 500 °C. The synthesized catalysts are denoted as M<sub>x</sub>C<sub>y</sub>Z<sub>z</sub>, where x, y and z represent the atomic concentration of alkaline-earth metal, Cu and Zr, respectively. The sum of atomic concentration of metal was taken as 1.0, and a constant atomic concentration of Cu (0.5) was employed in this study.

### 2.2 Catalyst characterization

The X-ray diffraction (XRD) analysis of the sample was carried out on a PANalytical X'Pert diffractometer using nickel-filtered Cu K $\alpha$  radiation at 40 kV and 40 mA. Two theta angles ranged from 10 to 70° with a speed of 6° per minute.

The BET surface area ( $S_{BET}$ ) of sample was determined by a Micromeritics ASAP2020 M+C adsorption apparatus with nitrogen adsorption/desorption isotherms. Before each analysis, samples were dried at 200 °C under vacuum for 3 h.

Copper surface area ( $S_{Cu}$ ) in the reduced catalyst was determined using the N<sub>2</sub>O titration method similar to that described by Chinchén et al.<sup>25</sup>. The catalyst (0.2 g) was reduced in an H<sub>2</sub>/He mixture at 300 °C for 1 h. Then, it was purged with He and cooled to 60 °C. A flow of 1 vol% N<sub>2</sub>O/He gas mixture was fed into the reactor. The N<sub>2</sub> produced by the decomposition of N<sub>2</sub>O on the exposed Cu atoms was detected using a mass spectrometer (Pfeiffer Vacuum Quadstar, 32-bit). The copper surface area was calculated assuming an atomic copper surface density of  $1.46 \times 10^{19}$  Cu atoms/m<sup>2</sup> and a molar stoichiometry of N<sub>2</sub>O/Cu=0.5<sup>7</sup>.

Temperature-programmed reduction (TPR) measurements were performed in a linear quartz microreactor fed with a 10 vol% H<sub>2</sub>/N<sub>2</sub> mixture flowing at 50 ml/min and heated at a rate of 5 °C/min. A ca. 30-mg of a freshly calcined catalyst was placed on top of glass wool in the reactor. The outlet of the reactor was connected to a glass column packed with molecular sieve 5 Å in order to remove the moisture produced from reduction. The amount of consumed H<sub>2</sub> was measured by a thermal conductivity detector (TCD).

The surface electronic states were investigated by X-ray photoelectron spectroscopy (XPS, ESCALAB 250Xi, Thermo Scientific Escalab) with Al K $\alpha$  (1486.6 eV) radiation as the X-ray excitation source. All the binding energy values were calibrated by using C 1s = 284.8 eV as a reference.

The basicity of the catalysts was measured by CO<sub>2</sub> temperature-programmed desorption (CO<sub>2</sub>-TPD). Prior to the adsorption of CO<sub>2</sub>, the catalysts were reduced at 300 °C for 60 min in a flow of 10% H<sub>2</sub>/N<sub>2</sub> mixture. After cooling to room temperature, the catalyst was saturated with CO<sub>2</sub> at 50 °C for 60 min, and then flushed with He flow to remove any physisorbed molecules. Afterward, the TPD experiment was started with a heating rate of 5 °C/min under He flow, and the desorbed CO<sub>2</sub> was detected by a mass spectrometer. The amount of the desorbed CO<sub>2</sub> was quantified by comparing the integrated area

of the TPD curves to the peak area of the injected CO<sub>2</sub> calibration pulse.

### 2.3 Catalytic testing

Catalytic activity and selectivity tests for methanol synthesis from CO<sub>2</sub> hydrogenation were carried out in a continuous-flow, fixed-bed reactor. Prior to the catalytic measurements, the fresh catalyst was reduced in a stream of 10 vol% H<sub>2</sub>/N<sub>2</sub> at 300 °C for 3 h under atmospheric pressure. Then the reactor was cooled to 180 °C and the reactant gas (CO<sub>2</sub>:H<sub>2</sub>=1:3, molar) flow was introduced, raising the pressure to 3.0 MPa and the temperature to a given temperature. The transfer line from the reactor to the chromatograph was heated at 140 °C in order to avoid condensation of the reaction products. Effluent products were analyzed on-line with a gas chromatograph (6820, Agilent). The gases CO<sub>2</sub>, CO and the internal standard N<sub>2</sub> were analyzed using a thermal conductivity detector (TCD); organic products were analyzed with a flame ionization detector (FID). Conversion and selectivity values were calculated by mass-balance methods and the steady-state values were quoted as the average of four different analyses taken after 5 h on stream operation.

## 3. Results and Discussion

### 3.1 Textural and structural properties of the catalysts

The XRD spectra of CuO-ZrO<sub>2</sub> catalysts doped with different alkaline-earth oxides (5 mol%) were shown in Fig.1 (A). The diffraction peaks at  $2\theta$  of 35.6° and 38.8° are ascribed to the CuO phase (JCPDS 80-1268), and the diffraction peak of  $2\theta=30.3^\circ$  is assigned to the tetragonal ZrO<sub>2</sub> (*t*-ZrO<sub>2</sub>, JCPDS, 88-1007). Furthermore, two small peaks for monoclinic ZrO<sub>2</sub> (*m*-ZrO<sub>2</sub>,  $2\theta=28.2^\circ$ ,  $31.5^\circ$ , JCPDS 83-0940) can be detected on the undoped CuO-ZrO<sub>2</sub> sample. With the introduction of alkaline-earth oxides, the diffraction peaks of CuO and *t*-ZrO<sub>2</sub> become weaker and broader, which indicates that the alkaline-earth oxides hinder the crystallization of CuO and ZrO<sub>2</sub> in catalysts, and such an effect increases in the order MgO < CaO < SrO < BaO. The average particle size of CuO was calculated with Scherer equation. As can be seen from Table 1, the particle size of CuO decreases progressively from MgO-doped to BaO-doped sample. There is no diffraction peaks of alkaline-earth oxides crystallites for all the investigated samples, as shown in Fig. 1 (A). The reason for this is ascribed to the formation of non-crystalline MZrO<sub>3</sub> (M= Mg, Ca, Sr, Ba) compound, which could not be detected by XRD technique due to the low degree of crystallization. The crystalline MZrO<sub>3</sub> compounds can be detected with a high calcination temperature for the samples<sup>26</sup>.

Fig. 1 (B) shows the XRD patterns of CuO-ZrO<sub>2</sub> catalysts with different MgO contents. It can be seen that the diffraction peak intensity of CuO and ZrO<sub>2</sub> decline with increasing MgO concentration. A similar variation trend was observed for the average particle size of CuO, as shown in Table 1. An enlarged view of the diffraction peaks of CuO and ZrO<sub>2</sub> components in

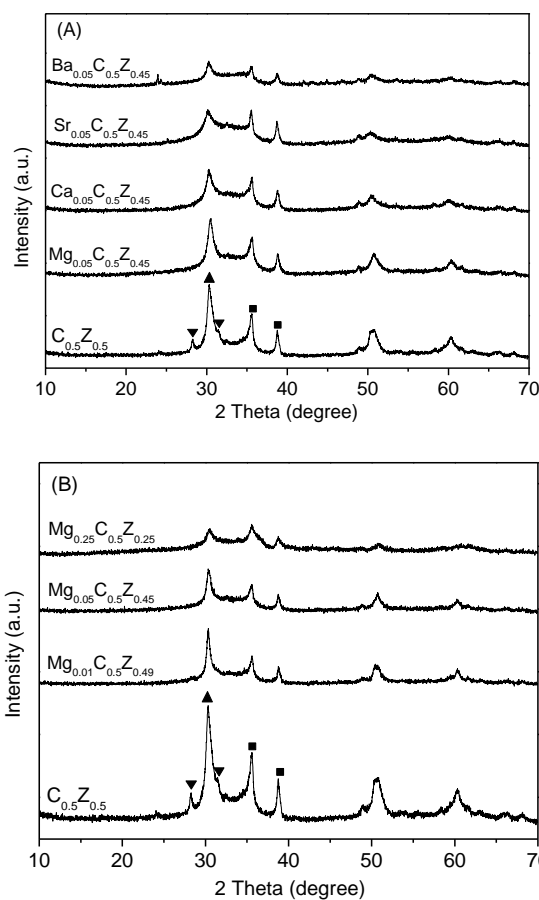


Fig. 1. XRD patterns of CuO-ZrO<sub>2</sub> catalysts doped with different alkaline-oxide (A) and with different amount of MgO (B). (■) CuO; (▲) ZrO<sub>2</sub> (tetragonal); (▼) ZrO<sub>2</sub> (monoclinic).

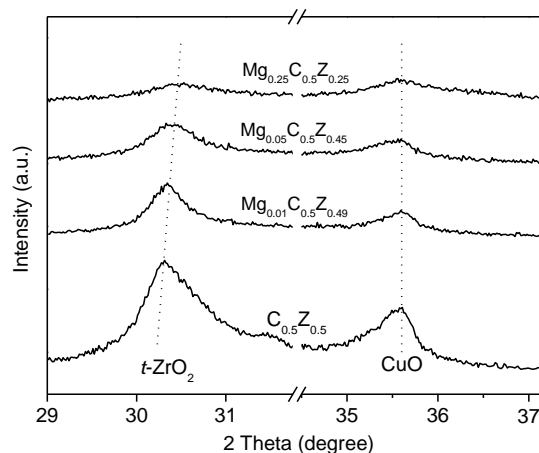


Fig. 2. Magnification XRD patterns of *t*-ZrO<sub>2</sub> and CuO phase in CuO-ZrO<sub>2</sub> catalysts with different MgO contents.

MgO-doped CuO-ZrO<sub>2</sub> catalyst was presented in Fig. 2. With the introduction of MgO, the diffraction peak of *t*-ZrO<sub>2</sub> shifts toward higher  $2\theta$  angle. This is an indicative of a decrease in the crystal lattice parameter, which is resulted from the

substitution of  $Zr^{4+}$  (radius 0.72 Å) by  $Mg^{2+}$  cations (radius 0.65 Å)<sup>27</sup>. However, there is no shift of CuO diffraction peak after MgO doping. These results further confirmed that  $Mg^{2+}$  was incorporated into  $ZrO_2$  lattice rather than CuO lattice.

The BET surface areas derived from nitrogen physisorption are listed in Table 1. A marked increase in  $S_{BET}$  was observed for MgO-doped CuO- $ZrO_2$  catalyst, whereas the increase was not notable for CaO-, SrO-, and BaO-doped samples. Copper surface area, which is determined by  $N_2O$  titration, is also presented in Table 1. Obviously, the incorporation of alkaline-earth oxides lead to an increase in  $S_{Cu}$  in the order  $MgO < CaO < SrO < BaO$ . In the case of MgO-doped samples, the value of  $S_{Cu}$  increases continually with increasing MgO doping content, and a maximum of 15.2  $m^2/g$  is obtained over  $Mg_{0.25}C_{0.5}Z_{0.25}$  sample. The variation of  $S_{Cu}$  is in accordance with the results regarding CuO crystallite size, as determined from XRD.

Table 1. Physicochemical properties of the CuO- $ZrO_2$  catalysts doping with alkaline-earth oxides

sample	$S_{BET}$ ( $m^2/g$ )	CuO crystallite size (nm) <sup>a</sup>	$S_{Cu}$ ( $m^2/g$ ) <sup>b</sup>
$C_{0.5}Z_{0.5}$	35.7	22.9	2.8
$Mg_{0.05}C_{0.5}Z_{0.45}$	45.8	21.0	7.4
$Ca_{0.05}C_{0.5}Z_{0.45}$	37.8	20.8	8.0
$Sr_{0.05}C_{0.5}Z_{0.45}$	37.1	20.8	8.3
$Ba_{0.05}C_{0.5}Z_{0.45}$	36.4	20.3	10.6
$Mg_{0.01}C_{0.5}Z_{0.49}$	39.1	21.7	4.4
$Mg_{0.03}C_{0.5}Z_{0.47}$	45.3	21.2	6.2
$Mg_{0.1}C_{0.5}Z_{0.4}$	46.4	21.2	13.7
$Mg_{0.25}C_{0.5}Z_{0.25}$	56.2	16.2	15.2

<sup>a</sup> Determined by XRD. <sup>b</sup> Determined by  $N_2O$  titration at 60 °C.

### 3.2 The surface oxidation states of catalyst

The surface oxidation states of CuO- $ZrO_2$  and alkaline-earth oxides doped CuO- $ZrO_2$  catalysts were investigated by XPS. As shown in Table 2, the binding energies (BE) of Cu 2 $p_{3/2}$  are in the range of 933.7-934.2 eV for all the catalysts, suggesting that the chemical state of copper is  $Cu^{2+}$ <sup>18</sup>. With the introduction of alkaline-earth oxide, a slight shift towards lower BE of Cu 2 $p_{3/2}$  was observed. The BE value of ca. 181.8 eV measured for Zr 3 $d_{5/2}$  indicates the presence of zirconium oxide

Table 2 Binding energies of the core electrons for CZ and MCZ (M= Mg, Ca, Sr and Ba) catalysts determined by XPS

Catalyst	Binding Energy (eV)		
	Cu 2 $p_{3/2}$	Zr 3 $d_{5/2}$	M
CZ	934.2	181.9	-
$Mg_{0.05}C_{0.5}Z_{0.45}$	934.0	181.8	Mg 1s: 1304.8
$Ca_{0.05}C_{0.5}Z_{0.45}$	933.8	181.8	Ca 2 $P_{3/2}$ : 346.9
$Sr_{0.05}C_{0.5}Z_{0.45}$	933.7	181.8	Sr 3 $d_{5/2}$ : 133.2
$Ba_{0.05}C_{0.5}Z_{0.45}$	933.7	181.8	Ba 3 $d_{5/2}$ : 780.1

with an oxidation state of +4<sup>11</sup>. There is no significant change in the BE value of Zr with the incorporation of alkaline-earth oxide. Furthermore, the BE values of alkaline-earth metal (Mg, Ca, Sr and Ba) in the catalysts are very close to those of the corresponding oxide (MgO, CaO, SrO and BaO), which

discloses that the alkaline-earth metal exist in a cationic state<sup>11,28</sup>.

### 3.3 The reducibility of catalyst

In order to investigate the reduction behavior of the catalysts,  $H_2$ -TPR measurements were carried out. Fig. 3 (A) shows the TPR profiles of CuO- $ZrO_2$  catalysts doped with different alkaline-earth oxides. For comparison, the TPR profile of the unsupported CuO powder is also presented. All samples exhibit

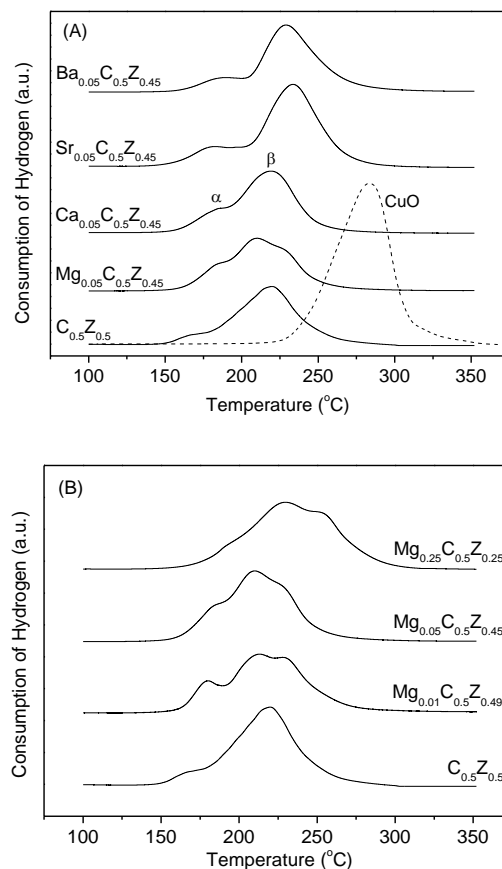


Fig. 3.  $H_2$ -TPR profiles of CuO- $ZrO_2$  catalysts doped with different alkaline-oxide (A) and with different amount of MgO (B).

Table 3 Temperature of reduction peaks over CuO- $ZrO_2$  catalysts doping with alkaline-earth oxides

Catalyst	$T_\alpha$ (°C)	$T_\beta$ (°C)	$T_\gamma$ (°C)
$C_{0.5}Z_{0.5}$	175	220	-
$Mg_{0.05}C_{0.5}Z_{0.45}$	183	208	228
$Ca_{0.05}C_{0.5}Z_{0.45}$	185	219	-
$Sr_{0.05}C_{0.5}Z_{0.45}$	186	234	-
$Ba_{0.05}C_{0.5}Z_{0.45}$	190	229	-
$Mg_{0.01}C_{0.5}Z_{0.49}$	179	213	228
$Mg_{0.25}C_{0.5}Z_{0.25}$	205	229	253

two reduction peaks, with the exception of MgO-doped CuO- $ZrO_2$  catalyst. As well documented, the low temperature peak ( $\alpha$  peak) is attributed to the reduction of highly dispersed CuO

surface species, and the peak appearing at higher temperature ( $\beta$  peak) is due to the reduction of bulk-like CuO<sup>7,29,30</sup>. In addition, as shown in Fig. 3 (A), the reduction temperature of CuO in  $C_{0.5}Zr_{0.5}$  sample is much lower than that of the unsupported CuO (*ca.* 285 °C). This result reveals that  $ZrO_2$  can facilitate the reduction of CuO via the interaction between them, a fact that is consistent with previous observations<sup>31-34</sup>. Table 3 summarizes the temperatures of reduction peaks for the investigated catalysts. Compared with the undoped CuO-ZrO<sub>2</sub> sample, both  $\alpha$  and  $\beta$  peak shift toward higher temperature with the introduction of CaO, SrO and BaO. This indicates that the incorporation of alkaline-earth oxides weakens the interaction between CuO and  $ZrO_2$ , which results in a decrease in the reducibility of CuO. As far as the MgO-doped CuO-ZrO<sub>2</sub> catalyst is concerned, the peak appearing in the higher-temperature region splits into two parts, which are denoted as  $\beta$  and  $\gamma$  peak. A similar observation of the multiple TPR peaks for the bulk-like CuO was reported by Wang et al.<sup>32</sup>. The split of the reduction peak is originated from the difference in the interaction strength, and  $\gamma$  peak corresponds to the reduction of CuO interacting with  $ZrO_2$  weakly. As shown in Table 3, the temperature of reduction peak of MgO-doped catalyst is much lower than that of SrO- and BaO-doped samples. For example, the temperature of  $\beta$  peak of  $Sr_{0.05}C_{0.5}Zr_{0.45}$  is 234 °C; while that of  $\beta$  and  $\gamma$  peak are 208 and 228 °C for  $Mg_{0.05}C_{0.5}Zr_{0.45}$ , respectively. These results suggest that a smaller effect of doping on the reducibility of CuO is obtained for the MgO-doped CuO-ZrO<sub>2</sub> catalyst.

Fig. 3 (B) shows the influence of MgO content on the reduction behavior of CuO-ZrO<sub>2</sub> catalyst. The change in the reduction temperature of CuO is insignificant from  $Mg_{0.01}C_{0.5}Zr_{0.49}$  to  $Mg_{0.05}C_{0.5}Zr_{0.45}$  sample. However, as the content of MgO reached 25 mol%, the increase in the reduction temperature become distinct. The variation of reduction temperature is also related to the interaction between CuO and  $ZrO_2$ , which decreases drastically when excessive MgO is added.

### 3.4 The basicity of the catalysts

The surface base properties of catalysts were investigated by CO<sub>2</sub>-TPD technique, and the CO<sub>2</sub> desorption profiles obtained for CuO-ZrO<sub>2</sub> and alkaline-earth oxides doped CuO-ZrO<sub>2</sub> catalysts are presented in Fig. 4 (A). A desorption peak with a maximum at *ca.* 105 °C was observed for all investigated samples. However, the TPD profile is highly asymmetric with a tail towards higher temperature, which is the result of a complex overlapping of several CO<sub>2</sub> desorption processes arising from different basic sites. In general, the basicity of metal oxide can be divided into three categories (weak, medium, and strong) according to the strength of base site<sup>35,36</sup>. The weak basic sites are related to the surface hydroxyl group; the medium basic sites are ascribed to the metal-oxygen pairs, i.e.  $Zr^{4+}-O^{2-}$  pair in this case; the strong basic sites are associated with the low-coordination oxygen anions<sup>19,36</sup>. Unfortunately, attempts at deconvolution of the TPD spectrum into three peaks were unsuccessful in this case. To facilitate discussion, CO<sub>2</sub>-

TPD profiles are roughly divided into three regions<sup>37,38</sup>: 50-150 °C, 150-240 °C and > 240 °C, which correspond to CO<sub>2</sub> desorption of weak, medium and strong site, respectively. The number of different base site was evaluated by calculating the integral of each region, and the data were summarized in Table 4. It can be seen that the number of total basic sites of alkaline-earth oxides doped samples is higher than that of undoped CuO-ZrO<sub>2</sub>. Moreover, the contributions of single basic site to the total basic sites was calculated and listed in Table 4. The fractions of the strong basic site increased in the order  $C_{0.5}Zr_{0.5} < Mg_{0.05}C_{0.5}Zr_{0.45} < Ca_{0.05}C_{0.5}Zr_{0.45} < Sr_{0.05}C_{0.5}Zr_{0.45} < Ba_{0.05}C_{0.5}Zr_{0.45}$ , whereas a contrary trend was obtained for the weak basic site. As for the contributions of medium basic sites to total basic sites, no apparent change is observed for all investigated catalysts. It is noteworthy that, as shown in Fig 4(A), the upper temperature limit of desorption profile increases progressively from  $C_{0.5}Zr_{0.5}$  to  $Ba_{0.05}C_{0.5}Zr_{0.45}$  sample, suggesting a continuous increase in the strength of strong basic sites. For instance, the CO<sub>2</sub> desorption over  $C_{0.5}Zr_{0.5}$  occurs at a temperature below 300 °C, while the desorption curve of  $Ba_{0.05}C_{0.5}Zr_{0.45}$  extend up to 450 °C. The variation of the strength of basic sites is related to the substitution of  $Zr^{4+}$  by the alkaline-earth cations. As stated above, the basicity of strong basic sites is originated from the low-coordination oxygen anions; the greater an oxygen anion's

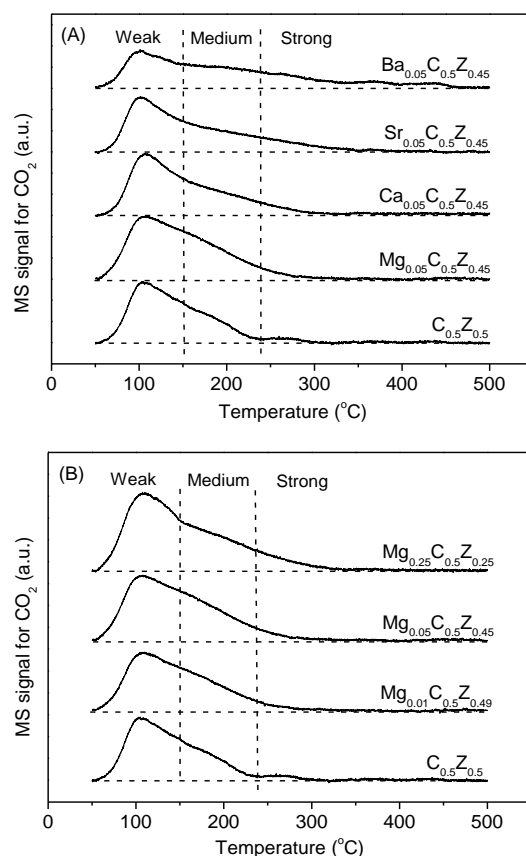


Fig. 4. CO<sub>2</sub>-TPD profiles of CuO-ZrO<sub>2</sub> catalysts doped with different alkaline-oxide (A) and with different amount of MgO (B).

electrodonating is, the stronger its Lewis basicity will be<sup>39,40</sup>. It is well known that the electronegativity of alkaline-earth cations is smaller than that of  $Zr^{4+}$  and decreases in the order  $Mg^{2+} < Ca^{2+} < Sr^{2+} < Ba^{2+}$ . Therefore, the electrodonating property of oxygen anions neighboring  $Zr^{4+}$  enhance with the partial substitution of  $Zr^{4+}$  by alkaline-earth cations, leading to the increase in the strength of basic sites.

Fig. 4 (B) shows the  $CO_2$ -TPD curves of CuO-ZrO<sub>2</sub> catalysts doped with different MgO content. The TPD curve extends to a higher temperature with increasing the amount of MgO doping, which also indicates an enhancement in the strength of strong basic sites. Furthermore, as shown in Table 4, the increase in MgO doping give rise to an increase in the fractions of the strong basic site.

Table 4 The basicity and the distribution of basic sites over CuO-ZrO<sub>2</sub> catalysts doping with alkaline-earth oxides

Catalyst	Number of basic sites ( $\mu\text{mol/g}$ ) and contribution <sup>a</sup> (%)			
	Weak	Medium	Strong	Total
$C_{0.5}Z_{0.5}$	12.6(64.4)	6.4 (32.6)	0.6 (3.0)	19.6
$Mg_{0.05}C_{0.5}Z_{0.45}$	14.2(58.1)	9.2 (37.6)	1.0 (4.3)	24.4
$Ca_{0.05}C_{0.5}Z_{0.45}$	12.2(56.7)	7.7 (36.0)	1.6 (7.3)	21.5
$Sr_{0.05}C_{0.5}Z_{0.45}$	11.1(53.6)	6.8 (33.1)	2.7 (13.3)	20.6
$Ba_{0.05}C_{0.5}Z_{0.45}$	8.0 (39.9)	6.5 (32.4)	5.6 (27.7)	20.1
$Mg_{0.01}C_{0.5}Z_{0.49}$	12.2(59.0)	7.7 (37.4)	0.7 (3.6)	20.6
$Mg_{0.25}C_{0.5}Z_{0.25}$	16.4(55.8)	10.4 (35.4)	2.6(8.8)	29.4

<sup>a</sup> The number of weak, medium and strong sites expressed in the amount of desorbed  $CO_2$  at 50-150, 150-240 and  $>240$  °C, respectively. The value in the parenthesis is the fraction of single basic site to the number of total basic site.

### 3.5 Catalytic activity and selectivity

Activity and selectivity results for methanol synthesis from  $CO_2$  hydrogenation over the undoped and alkaline-earth oxides doped CuO-ZrO<sub>2</sub> catalysts are summarized in Table 5. Methanol and CO are the only carbon-containing products under the reaction conditions and traces of methane can be detected at high temperatures.

As illustrated in Table 5, the conversion of  $CO_2$  declined with the incorporation of CaO, SrO and BaO, and a catalytic activity sequence of  $C_{0.5}Z_{0.5} > Ca_{0.05}C_{0.5}Z_{0.45} > Sr_{0.05}C_{0.5}Z_{0.45} > Ba_{0.05}C_{0.5}Z_{0.45}$  was obtained. However, for the MgO-doped CuO-ZrO<sub>2</sub> sample, an increase in  $CO_2$  conversion was observed as the doping amount is no more than 10 mol%. A further increase in the doping amount of MgO results in a decrease in  $CO_2$  conversion. As well documented, the catalytic activity and the  $S_{Cu}$  in a reduced catalyst are strongly correlated, and a large value of  $S_{Cu}$  is favorable for a high catalytic activity for the hydrogenation of  $CO_2$ <sup>5,12,13,41,42</sup>. Obviously, the decrease in  $CO_2$  conversion over CaO-, SrO- and BaO-doped catalysts is contradictory to the above statement because the  $S_{Cu}$  increases significantly with the doping of alkaline-earth oxide, as shown in the part of 3.1. This can be explained as follows. According to the dual-site mechanism, the Cu component serves to dissociatively adsorb  $H_2$  and to provide a source of atomic

hydrogen by spillover. In fact, there are two steps involved in the process of dissociatively adsorb  $H_2$ . One is the adsorption of  $H_2$  over the Cu active site; the other is the dissociation of the adsorbed  $H_2$ . The results of  $H_2$ -TPR disclosed that the reducibility of CuO was depressed with the introduction of CaO, SrO and BaO. Since the reducibility of CuO reflect the easiness of the dissociation of adsorbed  $H_2$ , the decline in the reducibility of CuO implies that the adsorbed  $H_2$  over the resulting Cu sites become more difficult to dissociate. In other words, with the addition of CaO, SrO and BaO, the rate of producing atomic hydrogen decreases though more Cu active sites are available for  $H_2$  adsorption. As a result, compared to the undoped CuO-ZrO<sub>2</sub> catalyst, CaO-, SrO- and BaO-doped samples exhibit a lower  $CO_2$  conversion. Moreover, since the reducibility of CuO in catalyst decreases in a sequence of  $Ca_{0.05}C_{0.5}Z_{0.45} > Sr_{0.05}C_{0.5}Z_{0.45} > Ba_{0.05}C_{0.5}Z_{0.45}$ , the same sequence of the conversion of  $CO_2$  is obtained. For the MgO-doped samples, a remarkable increase in the copper surface area is observed; while the effects of the doping on the reducibility of CuO is much less than that of CaO-, SrO- and BaO-doped samples, as stated in the part of 3.3. Under such a condition, the copper surface area will be a predominant factor. Therefore, it can be understand that a small increase in the  $CO_2$  conversion is achieved when an appropriate amount of MgO is introduced into CuO-ZrO<sub>2</sub>. As the amount of MgO doping is 25 mol%, the decline in the reducibility of CuO will be significant, which results in a low conversion of  $CO_2$ , and a value of 8.8% is obtained on  $Mg_{0.25}C_{0.5}Z_{0.25}$  sample.

Table 5 Catalytic performance for hydrogenation of  $CO_2$  to methanol over Cu-ZrO<sub>2</sub> catalysts doping with alkaline-earth oxides

Catalyst	$CO_2$ conversion (%)	$CH_3OH$ selectivity (%)	$CH_3OH$ yield (%)
$C_{0.5}Z_{0.5}$	9.9	45.4	4.5
$Mg_{0.05}C_{0.5}Z_{0.45}$	10.6	50.9	5.4
$Ca_{0.05}C_{0.5}Z_{0.45}$	8.1	51.5	4.2
$Sr_{0.05}C_{0.5}Z_{0.45}$	5.9	52.7	3.1
$Ba_{0.05}C_{0.5}Z_{0.45}$	5.4	40.6	2.2
$Mg_{0.01}C_{0.5}Z_{0.49}$	9.8	49.0	4.8
$Mg_{0.05}C_{0.5}Z_{0.47}$	10.3	51.5	5.3
$Mg_{0.1}C_{0.5}Z_{0.4}$	10.5	51.3	5.4
$Mg_{0.25}C_{0.5}Z_{0.25}$	8.8	47.2	4.2

Experimental errors are within  $\pm 3\%$  of the values reported.

Reaction conditions: T=240 °C, P=3.0 MPa, GHSV=3600 h<sup>-1</sup>.

As also shown in Table 5, the methanol selectivity increases with the addition of MgO, CaO, and SrO. Various factors affecting the methanol selectivity have been proposed<sup>43-45</sup>. Recent investigation revealed that the surface basicity of the catalyst play a dominant role in determining the methanol selectivity, and the carbon containing intermediates adsorbed on the stronger basic site preferred to hydrogenate further to form methanol rather than dissociate to form CO<sup>18,19</sup>. The results of  $CO_2$ -TPD showed that both the strength and contribution of strong basic sites increased with the

introduction of alkaline-earth oxides. Therefore, MgO-, CaO-, and SrO-doped samples exhibit a higher methanol selectivity comparing to the undoped CuO-ZrO<sub>2</sub>. Nevertheless, the methanol selectivity decreases as BaO is incorporated into CuO-ZrO<sub>2</sub>. It is possible that the decline in methanol selectivity is related to the excessive basicity of BaO-doped sample, which will lower the activation and hydrogenation of the adsorbed intermediates. As the amount of MgO doping varies from 1 to 5 mol%, the change in the methanol selectivity (49.0-51.5%) is small because the change in the surface basicity of these catalysts is not significant, as can be seen from Fig.4 (B).

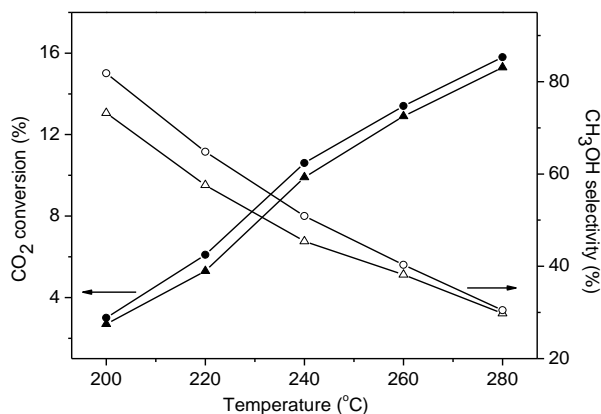


Fig. 5. Effect of temperature on the conversion of CO<sub>2</sub> (solid symbols) and selectivity of methanol (open symbols) over C<sub>0.5</sub>Zr<sub>0.5</sub> (triangles) and Mg<sub>0.05</sub>C<sub>0.5</sub>Zr<sub>0.45</sub> (circles) catalysts. Reaction conditions: H<sub>2</sub>/CO<sub>2</sub>=3, P=3.0 MPa, GHSV=3600 h<sup>-1</sup>.

Table 5 shows the methanol yield over the undoped and alkaline-earth oxides doped CuO-ZrO<sub>2</sub>. The methanol yield increases with the doping of MgO, and a maximum of 5.4% was obtained over the Mg<sub>0.05</sub>C<sub>0.5</sub>Zr<sub>0.45</sub> sample. In comparison with the undoped CuO-ZrO<sub>2</sub>, the value increased by 20%. For the CaO-, SrO-, BaO-doped samples, the methanol yield is lower than that of undoped CuO-ZrO<sub>2</sub> catalyst, and a sequence of Ca<sub>0.05</sub>C<sub>0.5</sub>Zr<sub>0.45</sub> > Sr<sub>0.05</sub>C<sub>0.5</sub>Zr<sub>0.45</sub> > Ba<sub>0.05</sub>C<sub>0.5</sub>Zr<sub>0.45</sub> is obtained. Furthermore, the effects of reaction temperature on the catalytic performances were investigated over the C<sub>0.5</sub>Zr<sub>0.5</sub> and Mg<sub>0.05</sub>C<sub>0.5</sub>Zr<sub>0.45</sub> catalysts. As shown in Fig. 5, with the elevation of reaction temperature, the conversion of CO<sub>2</sub> increases but the CH<sub>3</sub>OH selectivity decreases. Similar results can be found in the literature<sup>30,33</sup>. This variation can be explained in terms of thermodynamics and kinetics. The synthesis of methanol and the reverse water-gas shift (RWGS) are the two parallel reactions involved in the CO<sub>2</sub> hydrogenation process. The synthesis of methanol is an exothermic reaction, whereas the reaction of RWGS exhibits endothermic character<sup>7,19</sup>. According to the thermodynamic principle, raising temperature is favorable for the formation of CO via the RWGS reaction. On the other hand, in comparison with methanol synthesis, the RWGS reaction has a higher apparent activation energy<sup>33,46</sup>, which means that the increase in CO production is faster than that of methanol with the increase in temperature. Consequently,

the CH<sub>3</sub>OH selectivity decreases along with the elevation of reaction temperature.

#### 4. Conclusions

CuO-ZrO<sub>2</sub> catalysts doped with alkaline-earth oxides were prepared and used for methanol synthesis from CO<sub>2</sub> hydrogenation. The effects of alkaline-earth oxides on the physicochemical and catalytic properties of catalysts were investigated. Based on the results of this work, the following conclusions can be made:

- 1 The introduction of alkaline-earth oxides hinders the crystallization of CuO and ZrO<sub>2</sub> components in CuO-ZrO<sub>2</sub> catalyst and improves the copper surface area as well as the BET surface area.
- 2 The incorporation of alkaline-earth oxides gives rise to a decrease in the interaction between CuO and ZrO<sub>2</sub> and further a declination in the reducibility of CuO.
- 3 Both the strength and the contribution of strong basic site increase with the addition of alkaline-earth oxides.
- 4 The conversion of CO<sub>2</sub> depends not only on the copper surface area but also on the reducibility of CuO in catalyst, and the latter play a predominant role in methanol synthesis over CaO-, SrO- and BaO-doped CuO-ZrO<sub>2</sub> catalyst. The increase in methanol selectivity correlate with the increase in the strength and the contribution of strong basic sites.
- 5 A suitable amount of MgO in CuO-ZrO<sub>2</sub> is beneficial for the catalytic activity and methanol selectivity, and a maximum methanol yield is obtained as the content of MgO doping is 5 mol%.

#### Acknowledgements

The authors thank Shanghai Municipal Education Commission (No. 13YZ117), Shanghai Municipal Science and Technology Commission (No. 13ZR1441200) and the National Natural Science Foundation of China (No. 21273150) for financial support.

#### Notes and references

- 1 C. Song, *Catal. Today*, 2006, **115**, 2.
- 2 W. Wang, S.P. Wang, X.B. Ma, J.L. Gong, *Chem. Soc. Rev.*, 2011, **40**, 3703.
- 3 G.A. Olah, A. Goepfert, G.K.S. Prakash, *J. Org. Chem.*, 2009, **74**, 487.
- 4 X.M. Liu, G.Q. Lu, Z.F. Yan, *Appl. Catal. A: Gen.*, 2005, **279**, 241.
- 5 F. Arena, K. Barbera, G. Italiano, G. Bonura, L. Spadaro, F. Frusteri, *J. Catal.*, 2007, **249**, 185.
- 6 R.A. Köppel, C. Stöcker, A. Baiker, *J. Catal.*, 1998, **179**, 515.
- 7 X.M. Guo, D.S. Mao, G.Z. Lu, S. Wang, G.S. Wu, *J. Catal.*, 2010, **271**, 178.
- 8 X.M. Guo, D.S. Mao, S. Wang, G.S. Wu, G.Z. Lu, *Catal. Commun.*, 2009, **10**, 1661.
- 9 R. Raudaskoski, M.V. Niemelä R.L. Keiski, *Top. Catal.*, 2007, **45**, 57.

- 10 M. Kilo, J. Weigel, A. Wokaun, R.A. K€oppel, A. Stoeckli, A. Baiker, *J. Mol. Catal. A: Chem.*, 1997, **126**, 169.
- 11 J. Sloczyński, R. Grabowski, A. Kozłowska, P. Olszewski, M. Lachowska, J. Skrzypek, J. Stoch, *Appl. Catal. A: Gen.*, 2003, **249**, 129.
- 12 J. Sloczyński, R. Grabowski, P. Olszewski, A. Kozłowska, J. Stoch, M. Lachowska, J. Skrzypek, *Appl. Catal. A: Gen.*, 2006, **310**, 127.
- 13 S. Natesakhawat, J.W. Lekse, J.P. Baltrus, P.R. Ohodnicki Jr., B.H. Howard, X.Y. Deng, C. Matranga, *ACS Catal.*, 2012, **2**, 1667.
- 14 H.Y. Ban, C.M. Li, K. Asami, K. Fujimoto, *Catal. Commun.*, 2014, **54**, 50.
- 15 I.A. Fisher, A.T. Bell, *J. Catal.*, 1997, **172**, 222.
- 16 F. Arena, G. Italiano, K. Barbera, S. Bordiga, G. Bonura, L. Spadaro, F. Frusteri, *Appl. Catal. A: Gen.*, 2008, **350**, 16.
- 17 Q.J. Hong, Z.P. Liu, *Surf. Sci.*, 2010, **604**, 1869.
- 18 X.M. Guo, D.S. Mao, G.Z. Lu, S. Wang, G.S. Wu, *J. Mol. Catal. A: Chem.*, 2011, **345**, 60.
- 19 P. Gao, F. Li, H.J. Zhan, N. Zhao, F.K. Xiao, W. Wei, L.S. Zhong, H. Wang, Y.H. Sun, *J. Catal.*, 2013, **298**, 51.
- 20 P. Gao, F. Li, N. Zhao, F.K. Xiao, W. Wei, L.S. Zhong, Y.H. Sun, *Appl. Catal. A: Gen.*, 2013, **468**, 442.
- 21 W.Y. Zhang, H. Wang, W. Wei, Y.H. Sun, *J. Mol. Catal. A: Chem.*, 2005, **231**, 83.
- 22 L.M. Madeira, R.M. Mart ın-Aranda, F.J. Maldonado-H ıda, J.L.G. Fierro, M.F. Portela, *J. Catal.*, 1997, **169**, 469.
- 23 S.N. He, Y.J. Cui, Y.L. Yao, R.M. Fang, Z.H. Shi, M.C. Gong, Y.Q. Chen, *Acta Phys. Chim. Sin.*, 2011, **27**, 1157.
- 24 S.R. Jain, K.C. Adiga, V.R. Pai Verneker, *Combust. Flame*, 1981, **40**, 71.
- 25 G.C. Chinchin, C.M. Hay, H.D. Vandervell, K.C. Waugh, *J. Catal.*, 1987, **103**, 79.
- 26 R. Watanabe, Y. Saito, C. Fukuhara, *Appl. Catal. A: Gen.*, 2014, **482**, 344.
- 27 N.N. Das, J. Konar, M.K. Mohanta, S.C. Srivastava, *J. Colloid Interface Sci.*, 2004, **270**, 1.
- 28 F. Papa, P. Luminata, P. Osiceanu, R. Birjega, M. Akane, I. Balint, *J. Mol. Catal. A: Chem.*, 2011, **346**, 46.
- 29 G. Avgouropoulos, T. Ioannides, H. Matralis, *Appl. Catal. B: Enviro.*, 2005, **56**, 87.
- 30 Y.P. Zhang, J.H. Fei, Y.M. Yu, X.M. Zheng, *Energ. Conv. Manag.*, 2006, **47**, 3360.
- 31 N.F.P. Ribeiro, M.M.V.M. Souza, M. Schmal, *J. Power Sources*, 2008, **179**, 329.
- 32 L.C. Wang, Q. Liu, M. Chen, Y.M. Liu, Y. Cao, H.Y. He, K.N. Fan, *J. Phys. Chem. C.*, 2007, **111**, 16549.
- 33 I. Meli ın-Cabrera, M. L ıppez Granados, J.L.G. Fierro, *J. Catal.*, 2002, **210**, 273.
- 34 M.D. Rhodes, A.T. Bell, *J. Catal.*, 2005, **233**, 198.
- 35 Z. Liu, J.A. Cort ́s-Concepci ́n, M. Mustian, M.D. Amiridis, *Appl. Catal. A: Gen.*, 2006, **302**, 232.
- 36 V.K. D ́ez, C.R. Apestegu ́a, J.I. Di Cosimo, *Catal. Today*, 2000, **63**, 53.
- 37 S. Kuś, M. Otremba, A. T ́orz, M. Taniewski, *Appl. Catal. A: Gen.*, 2002, **230**, 263.
- 38 H. Wang, M.H. Wang, W.Y. Zhang, N. Zhao, W. Wei, Y.H. Sun, *Catal. Today*, 2006, **115**, 107.
- 39 H. Wang, M. H. Wang, S. G. Liu, N. Zhao, W. Wei and Y. H. Sun, *J. Mol. Catal. A: Chem.*, 2006, **258**, 308.
- 40 S.F. Xia, X.M. Guo, D.S. Mao, Z.P. Shi, G.S. Wu, G.Z. Lu, *RSC Adv.*, 2014, **4**, 51688.
- 41 M. Saito, T. Fujitani, M. Takeuchi, T. Watanabe, *Appl. Catal. A: Gen.*, 1996, **138**, 311.
- 42 Q. Sun, Y.L. Zhang, H.Y. Chen, J.F. Deng, D. Wu, S.Y. Chen, *J. Catal.*, 1997, **167**, 92.
- 43 S. Fujita, S. Moribe, Y. Kanamori, M. Kakudate, N. Takezawa, *Appl. Catal. A: Gen.*, 2001, **207**, 121.
- 44 J. Toyir, P.R. de la Piscina, J.L.G. Fierro, N. Homs, *Appl. Catal. B: Enviro.*, 2001, **34**, 255.
- 45 M.D. Rhodes, A.T. Bell, *J. Catal.*, 2005, **233**, 198.
- 46 J. Yoshihara, C.T. Campbell, *J. Catal.*, 1996, **161**, 776.